Doping Graphene Transistors Using Vertical Stacked Monolayer WS_2 Heterostructures Grown by Chemical Vapour Deposition

*Haijie Tan[1], Ye Fan[1], Youmin Rong[1], Ben Porter[1], Chit Siong Lau[1], Yingqiu Zhou[1], Zhengyu He[1], Shanshan Wang[1], Harish Bhaskaran[1], Jamie H. Warner[1]**

[1]Department of Materials, University of Oxford, Parks Road, Oxford, OX1 3PH, United Kingdom

*Jamie.warner@materials.ox.ac.uk;

Abstract

We study the interactions in graphene/WS_2 2D layered vertical heterostructures with variations in the areal coverage of graphene by the WS_2. All 2D materials were grown by chemical vapour deposition and transferred layer by layer. Photoluminescence (PL) spectroscopy of WS_2 on graphene showed PL quenching along with an increase in the ratio of exciton/trion emission, relative to WS_2 on SiO_2 surface, indicating a reduction in the n-type doping levels of WS_2 as well as reduced radiative recombination quantum yield. Electrical measurements of a total of 220 graphene field effect transistors with different WS_2 coverage showed double-Dirac points in the field effect measurements, where one is shifted closer towards the 0V gate neutrality position due to the WS_2 coverage. Photo-irradiation of the WS_2 on graphene region caused further Dirac point shifts, indicative of a reduction in the p-type doping levels of graphene, revealing that the photogenerated excitons in WS_2 are split across the heterostructure by electron transfer from WS_2 to graphene. Kelvin probe microscopy showed that regions of graphene covered with WS_2 had a smaller work function and supports the model of electron transfer from WS_2 to graphene. Our results demonstrate the formation of junctions within a graphene transistor through the spatial tuning of the work function of graphene using these 2D vertical heterostructures.

KEYWORDS: Graphene, WS_2, 2D crystals, surface transfer doping, heterostructures

Introduction

Two-dimensional (2D) van der Waals (vdW) crystals including graphene, boron nitride and transition metal dichalcogenides (TMDs) have been considered as promising candidates in a new generation of nano-electronics, with the potential to extend scaling limits of conventional silicon-based transistors.[1,2,3] Alongside their ultrathin nature, high mechanical strength due to covalent bonding and wide range of electronic properties, 2D vdW crystals also serve as promising building blocks for new flexible electronics and optoelectronic devices.[4,5] Forming heterojunctions of 2D vdW crystals is a common approach to modulate the electronic properties of the materials for device applications. These heterojunctions based on vdW interactions rather than covalent bonding are not limited by crystal lattice mismatch, offering a wider range of choices in materials systems. Furthermore, the lack of dangling bonds on the monolayer crystal surfaces also enables high quality, atomically regulated interfaces.[6]

The discovery of graphene in 2004 has led to a surge of research in the physical phenomena of 2D materials as well as their device functionalities.[7] The high charge mobility, strong and broadband adsorption per unit mass, excellent mechanical strength, flexibility and transparency of graphene makes it a promising material for transparent electrodes and ultrafast photodetectors.[8,9] Optoelectronic properties of TMDs such as WS_2 and MoS_2 have also been investigated due to their sizable and direct band gaps,[10–12] which are believed to complement graphene's absence of band gap. Multiple studies have investigated the device applications of graphene/TMD heterostructures by artificially stacking the 2D crystals. Reports on tunneling field effect transistors,[13] biosensors,[14] photodetectors and photovoltaic cells,[15,16] have demonstrated the unique electronic properties and enhanced light-matter interactions that the graphene/TMD heterojunctions could offer. Prior investigations have revealed optical and electronic properties of these graphene/TMD heterostructures. In particular, photoluminescence (PL) quenching on TMD and a n-dop-

ing effect on graphene were observed in the mechanically exfoliated 2D crystals.[17,18] Mechanically exfoliated samples are often free from polymer residue and this enables atomically sharp interfaces between each 2D crystal in the vertical heterostructure. However, the prospect of utilizing mechanically exfoliated samples in commercial applications is small, and this promotes the investigation of similar properties in all chemical vapour deposition (CVD) grown 2D material vertical heterostructures. 2D crystals grown by CVD normally show properties different from their pristine form due to unintentional doping during growth and transfer process. Obtaining atomically sharp 2D heterointerfaces is more challenging using CVD materials due to residues that may form during transfer. Thus exploring whether such strong interlayer coupling exists in these of vdW crystals grown by CVD is essential for large-scale manufacture and would warrant potential industrial applications for such heterostructures.

In the following, we demonstrate the fabrication of a p^+-p isotype junction on graphene channels utilizing the charge transfer in graphene/WS_2 heterostructure. The doping effect of graphene brought by WS_2 can be further tuned by illumination. Both graphene and WS_2 were grown using CVD method and a total of 220 devices were fabricated. We investigate the doping effect through examining the devices' electronic characteristics when altering the spatial coverage of WS_2 on graphene FETs. The observed surface transfer doping, unlike conventional doping methods of graphene that involves electrostatic modulation,[19–22] chemical interaction,[23] or intercalation,[24] relies on charge transfer between interfaces without introducing significant structural defects to the as-doped material.[25] This finding offers an alternative method to selectively and controllably tune the Fermi level of graphene regions that could potentially form lateral p-n junctions on graphene transistors using other 2D vdW crystals. The doping asymmetry at these junction interfaces are found to be essential for effective photoresponsivity in graphene.[8,26] The controllable doping of graphene proposed in our study may also facilitate researches on the mechanisms of photocurrent generation in graphene-based photodetectors.[27,28] As no additional gate voltage is required

in modulating the charge carrier density, the junctions created in our devices using graphene/TMD 2D heterostructure can therefore be applied in fully transparent and flexible photodetectors. [9]

Results and Discussion

Both graphene and WS_2 were grown by CVD methods using our previously reported approaches.[29,30] Graphene/WS_2 hybrid devices were made by transferring graphene onto a silicon chip with 300 nm oxide, pre-patterned with more than 500 pairs of Cr/Au pads that act as source and drain electrodes. The graphene is then patterned by electron-beam lithography and oxygen plasma etching into channels. A WS_2/PMMA film is subsequently transferred on top of the chip containing the graphene channels. As the CVD-grown WS_2 crystals are randomly distributed across the region, multiple WS_2 crystals are transferred directly onto the graphene channels, forming vertical heterostructures that have spatially different coverage amounts.

Figure 1a,d shows a SEM image and an optical microscopy image of the device consisting of graphene/WS_2 heterostructures. The WS_2 domain extends across the three different surfaces of SiO_2, graphene and gold. The spatial map of integrated PL signal from the monolayer WS_2 is shown in Figure 1e and shows quenching in regions where the WS_2 domain lies above the graphene channel and gold electrode. Photo-excited electrons on WS_2 are able to transfer to gold or graphene, resulting in a suppressed recombination process of excitons and the quenching of PL signal. This agrees well with previous reports on the quenching effects in metal-semiconductor interfaces of 2D crystals.[17,31] The quenching of PL is an indicator of good contact between graphene/WS_2 vertical stacks.

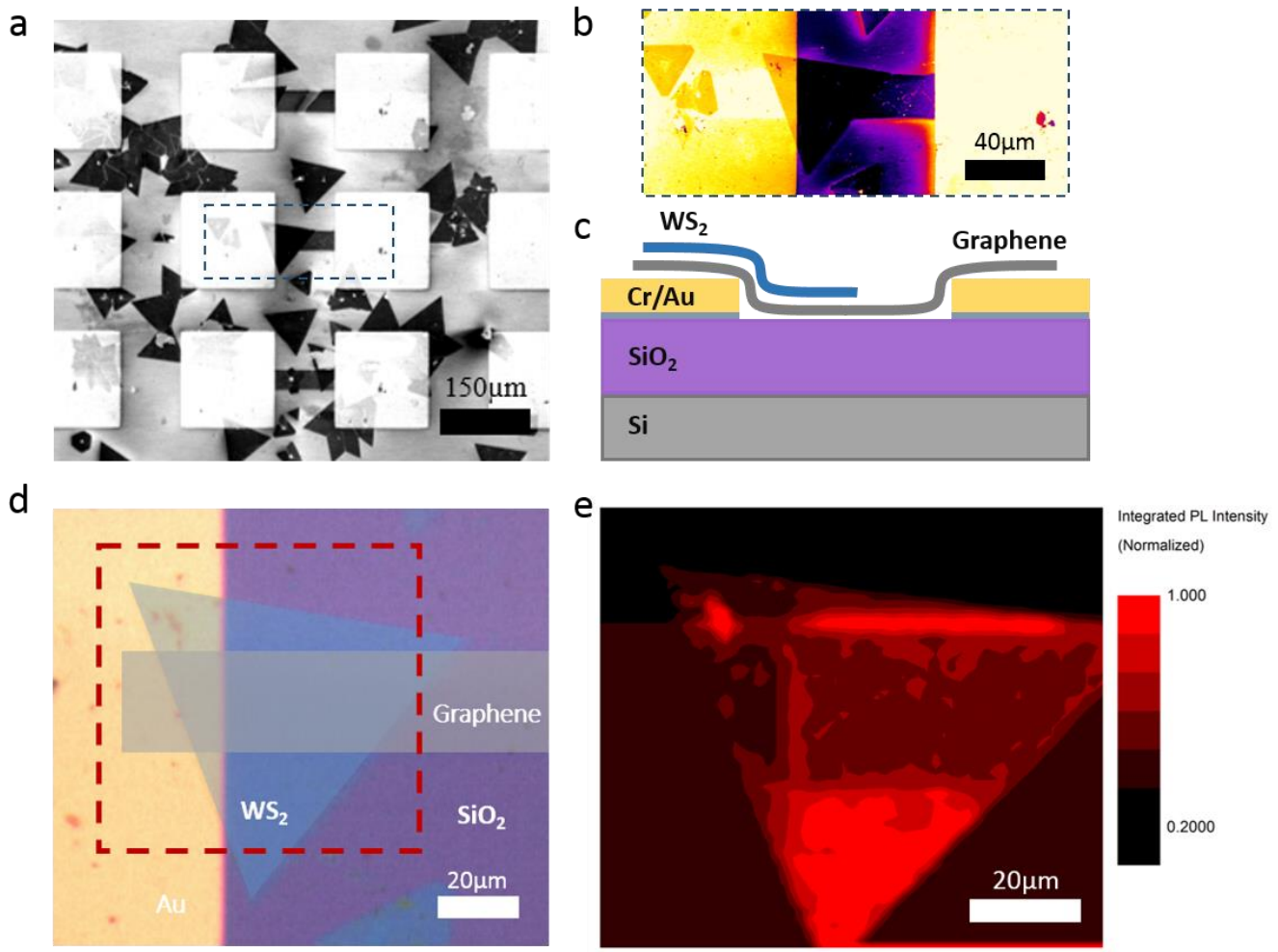

Figure 1. PL intensity spatial map of graphene/WS_2 heterostructure. (a) SEM image of devices with graphene channel and vertically stacked WS_2 crystals. Bright square regions are Cr/Au electrodes which are used as source/drain contacts of the graphene FETs. Dark triangular domains are WS_2 crystals. (b) SEM image with false colour of the region indicated in the blue dashed rectangle in (a). (c) Side view schematic of device structure. (d) Top view optical image of the graphene FET device with WS_2 partial coverage, with added colour overlay to help identify the different regions. (e) Spatial Map of the integrated PL intensity of WS_2 in the red dashed rectangle in (d).

Figure 2a shows the PL peak position map of the same hybrid device shown in Figure 1d. A blue shift of collected PL signal is observed when the WS2 domain lies above the graphene ribbons. The PL peak signals of WS_2 on graphene and SiO_2 substrates are plotted for further analysis. Using Lorentzian

fitting, the main peak of photoluminescence signal can be deconstructed into two separate peaks, attributed to the exciton (X) and negative trion (X^-) emission with corresponding photon energies of around 2.01 eV and 1.97 eV respectively. The energy difference of around 40 meV in the two peak positions is attributed to the binding energy of excitons to form negatively charged trion, which is consistent with previous reports of trion binding energy ranging from 20 to 40 meV.[32–34] For WS_2 on the graphene ribbons (i.e the vertical heterostructured region), the spectral weight of negative trion emission decreases relative to that of the exciton peak (Figure 2b), suggesting that electrons are depleted from WS_2 within the region.

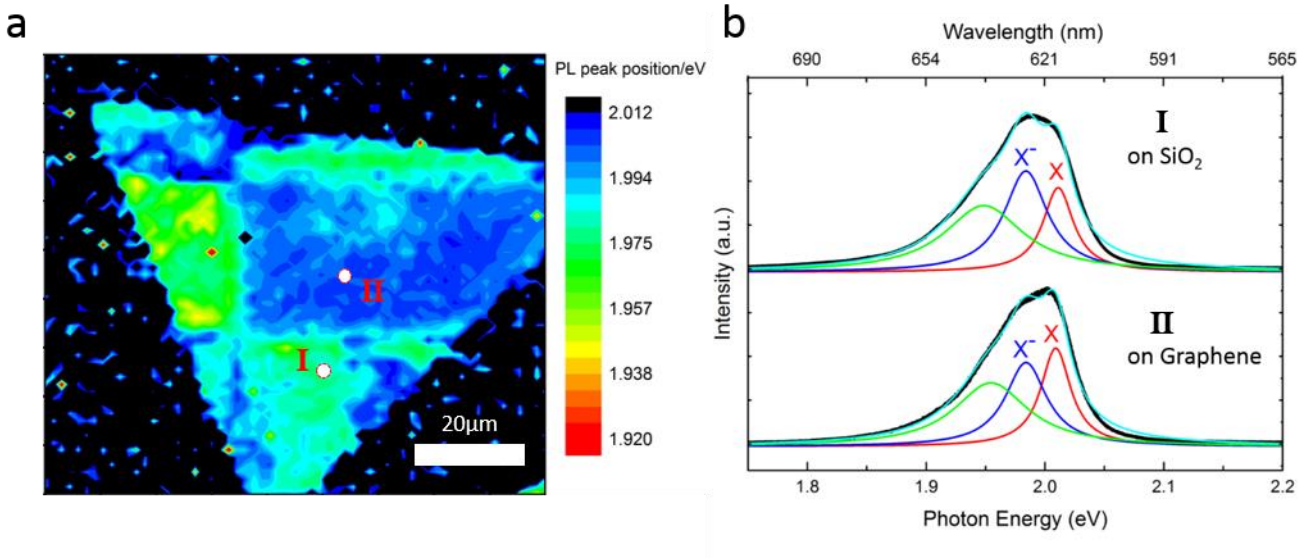

Figure 2. PL composition analysis of graphene/WS_2 heterostructure. (a) Spatial PL peak position map of WS_2 in heterostructure device. (b) PL spectra of WS_2 domain on Si substrate and graphene. Lorentzian fitting was used to decompose the PL peak to compare the spectral weight of negative trion (blue curve) and exciton (red curve).

The photoluminescence measurements in Figures 2 and 3 demonstrate the significant interaction between the WS_2 and graphene layer that should lead to changes in the local charge carrier densities. To explore this further we examine the electronic properties of field effect transistors. Figure 3 shows the field effect change in graphene channels for different levels of WS_2 coverage. The CVD-grown graphene on SiO_2 substrate has a Dirac point at around 70 V, which is typical for CVD graphene measured on SiO_2 in air and indicates p-doping. When graphene is partially covered by a WS_2 crystal, a second Dirac point

under a back gate potential of 20 V is observed. The appearance of two Dirac points in the gate sweeps suggests electron transfer from WS_2 to graphene, which reduces the level of p-doping of the graphene within the heterostructure region, forming a lateral separation on the graphene channel with different Fermi levels. When graphene is fully covered by WS_2 domains, the entire graphene channel has reduced p-doping compared to uncovered graphene and only one Dirac point is observed in the gate sweeps at much lower voltages.

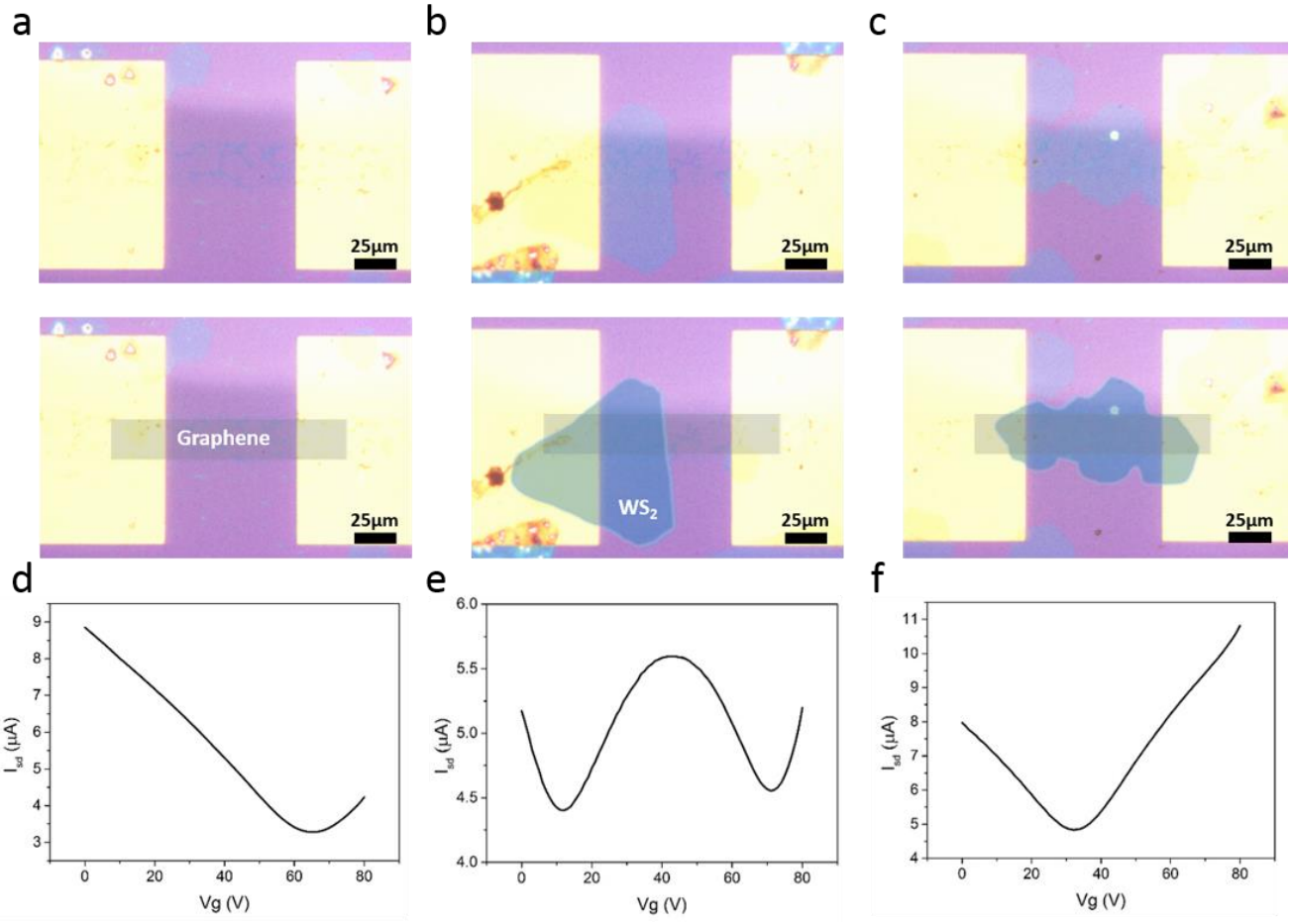

Figure 3. Gate dependence of graphene FETs. (a, b, c) Optical images with added schematic of 3 different types of graphene channels according to WS_2 coverage (no coverage, partial coverage and full coverage). (d,e,f) are corresponding field effect measurements of the different graphene transistors.

To further investigate the relationship of Dirac point positions and the coverage of WS_2 on graphene channels, we have studied a total of 220 graphene FET devices with variable WS_2 coverage. We

classify three different types of Graphene FETs, graphene channels without WS_2 coverage, graphene channels that are fully covered with WS_2, and graphene channels with partial WS_2 coverage. The average value of the Dirac point positions and the standard deviation are shown in Table 1. Compared with uncovered graphene channels and channels that are fully covered by WS_2 domains, graphene channels which are partially covered by WS_2 have corresponding Dirac points of around the same position at around 70 V and 20 V. This suggests that the difference in WS_2 coverage on graphene does not affect the positions of Dirac point significantly, but rather affects the relative weighting contribution of the two Dirac points in the gate sweeps. This can be interpreted using a simplified model of two resistors in series as shown in Figure 4a, where the overall channel resistance is the sum of the contact resistance and two laterally separated graphene regions, one covered with by WS_2 and the other without, expressed as R_w and R_g respectively. Figure 4b shows a schematic illustration of the band structures of these two graphene regions under different applied back gate potentials. The doped graphene reaches its neutrality point at around 20 V, transitions from p-type to a n-type transistor with increasing gate potential, while the uncovered graphene that is initially more p-doped reaches neutrality point at a larger back gate potential of around 70 V.

Table 1. Dirac point position of 3 types of graphene channels

Graphene channels	# of devices	Average Dirac point position (V)	σ (V)
No WS_2 coverage	93	70.9	6
Full WS_2 coverage	12	22.9	10.7
Partial WS_2 coverage (a)	115	76.9	8.9
Partial WS_2 coverage (b)	115	22.2	8.2

The device characteristics of channels with graphene/WS_2 heterostructure can be represented using a simplified model of two distinct graphene regions with different doping levels connected in series. The total channel resistance (R_T) of the graphene can thus be expressed using the equation $R_T = k \cdot R_w +$

$(1-k)\cdot R_g + R_C$, where k is the percentage of WS_2 coverage on graphene channel, R_C the contact resistance, and R_w, R_g the resistance of doped graphene covered by WS_2 and plain graphene respectively. To analyze the resistance of each regions of graphene, we introduce a model[21] to account for the electron-hole puddle density (Supporting Information section S2), in which the total charge carrier concentration is approximated using equation $n_T = \sqrt{{n_0}^2 + {n_G}^2}$, where n_0 is the residual carrier concentration and n_G is carrier concentration induced by a back-gated electric field. n_G can be further determined by the difference of the applied back-gate potential V_G and the position of graphene's charge neutrality point V_{CNP}, also known as Dirac point. The resistance of a region of graphene can be expressed as $R = \frac{L}{w}\cdot\frac{1}{\sigma} = \frac{L}{w}\cdot\frac{1}{e\cdot n\cdot\mu} = \frac{A}{\sqrt{1+(V_g-V_{CNP})^2/B^2}}$ where A, B are related to carrier mobility μ, and residual charge carrier density n_0. The excellent agreement between the measured channel gate-sweep characteristics and modelled curves shown in Figure 4f-h confirmed the local tuning of graphene's Fermi level due to transfer of electrons from WS_2 onto graphene.

The p-doping of CVD graphene has been commonly attributed to charge impurities unintentionally introduced by substrates, polymer residual and absorbents under ambient conditions.[35] Reports have shown that the encapsulation of graphene using TMDs and other 2D crystals remove the absorbed water molecules by a van der Waals self-cleaning process,[36,37] and thus a less p-doped graphene would be expected with transfer of WS_2 on graphene. However, this does not seem to be the main reason of the Dirac point shifting of graphene within the heterostructure. In the statistical analysis of charge carriers derived from the best fitting results of 115 graphene devices with double-Dirac points, we have found that the concentration of charge carriers of graphene under WS_2 domains is on average 1.85×10^{12} cm^{-2}, while graphene without WS_2 coverage has 1.15×10^{12} cm^{-2}. From the fitting results, we can conclude that the residual charge carrier density of graphene has in most cases increased after the stacking of WS_2 domains (Supporting Information Figure S2).This suggest that the main mechanism of the observed doping effect

is more likely to be an introduction of charge carriers rather than just a simple cleaning process with the removal of absorbed gas and water molecules, which would have resulted in a more pristine graphene with a lower residual charge carrier.

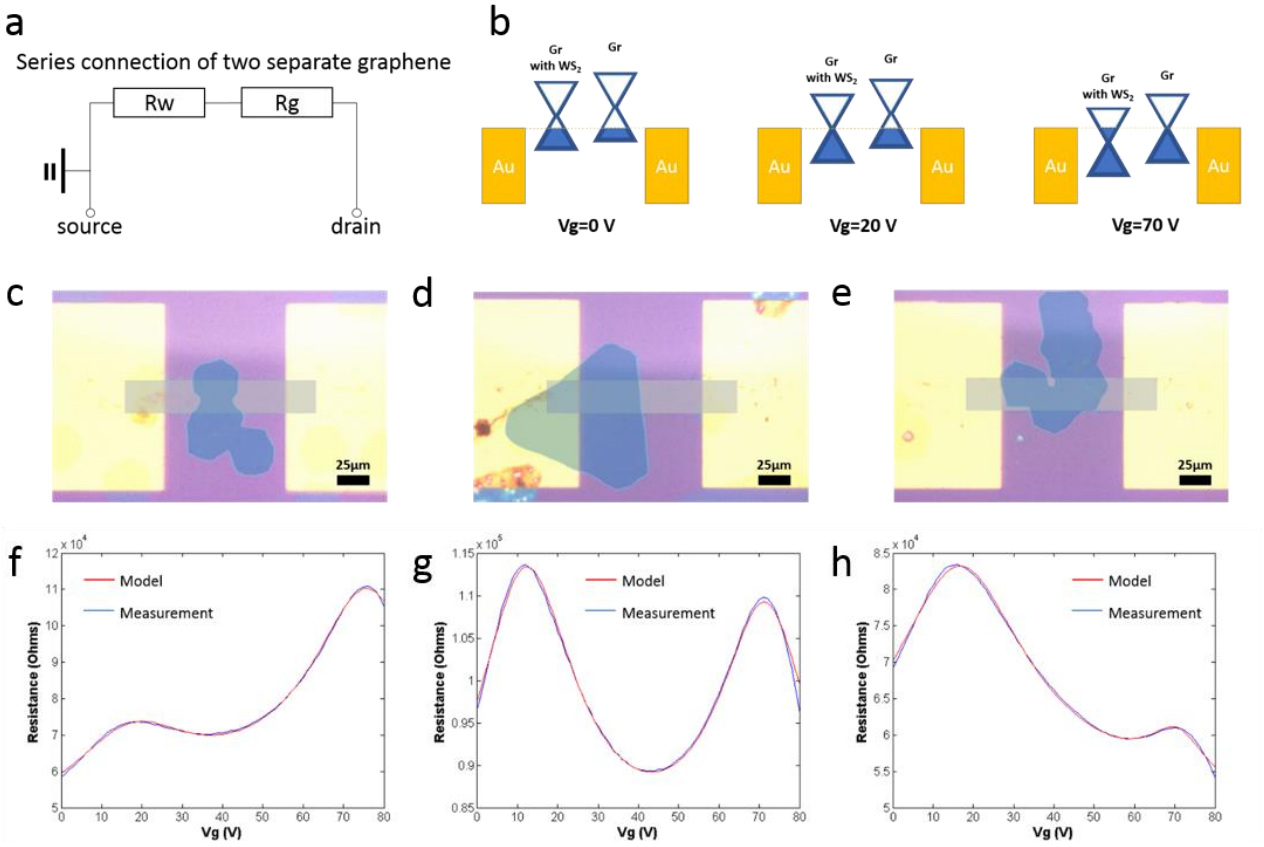

Figure 4. Electronic model of laterally separated graphene channel. (a) Simplified resistance model of graphene channel where R_w and R_g, which represent the resistance of doped and un-doped graphene respectively, are series connected within the transistor channel. (b) Schematic illustration of band structure of the two distinct graphene regions under different applied back gate potential. (c,d,e) Optical images with added schematic of graphene channels with 28%, 50% and 85% WS_2 coverage. (f,g,h) Corresponding field effect measurements and simulated resistance from electronic model.

The charge transfer that has taken place at the interface can also be reflected by the surface potential at the lateral isotype junction along the graphene transistor. Previous studies have reported using Kelvin Probe Microscopy (KPM) measurements to investigate the heterojunction as well as the doping effect

of graphene and TMDs[38–40]. During a KPM measurement, a direct current is applied to the sample to nullify the contact potential difference (CPD) between the KPM tip and the sample surface, thus a sample on a conductive substrate is required (Figure 5a). A representative energy band diagram at equilibrium state is shown in Figure 5b to demonstrate the relationship of the measured CPD work functions of the different surface. The difference in the vacuum level, denoted as E_{vac}, of the different materials is due to band bending when the charge transfer take place for their Fermi levels, denoted as $E_{F,}$ to align. CPD of the KPM tip and graphene or graphene/WS_2 heterostructure can thus be written as the difference in their work function, i.e., $CPD_{graphene} = \frac{\phi_{tip} - \phi_{graphene}}{e}$ for graphene and $CPD_{WS_2/graphene} = \frac{\phi_{tip} - \phi_{WS_2/graphene}}{e}$ for the heterostructured region, where ϕ_{tip}, $\phi_{graphene}$, $\phi_{WS_2/graphene}$ are work functions of the tip (Cr/Pt), graphene, and heterostructured region respectively. From Figure 5d and 5e, we find that the work function of the heterostructured region is smaller than graphene, which translates into a higher Fermi level before reaching equilibrium and reinforces our claim of the introduction of electrons to graphene from WS_2.

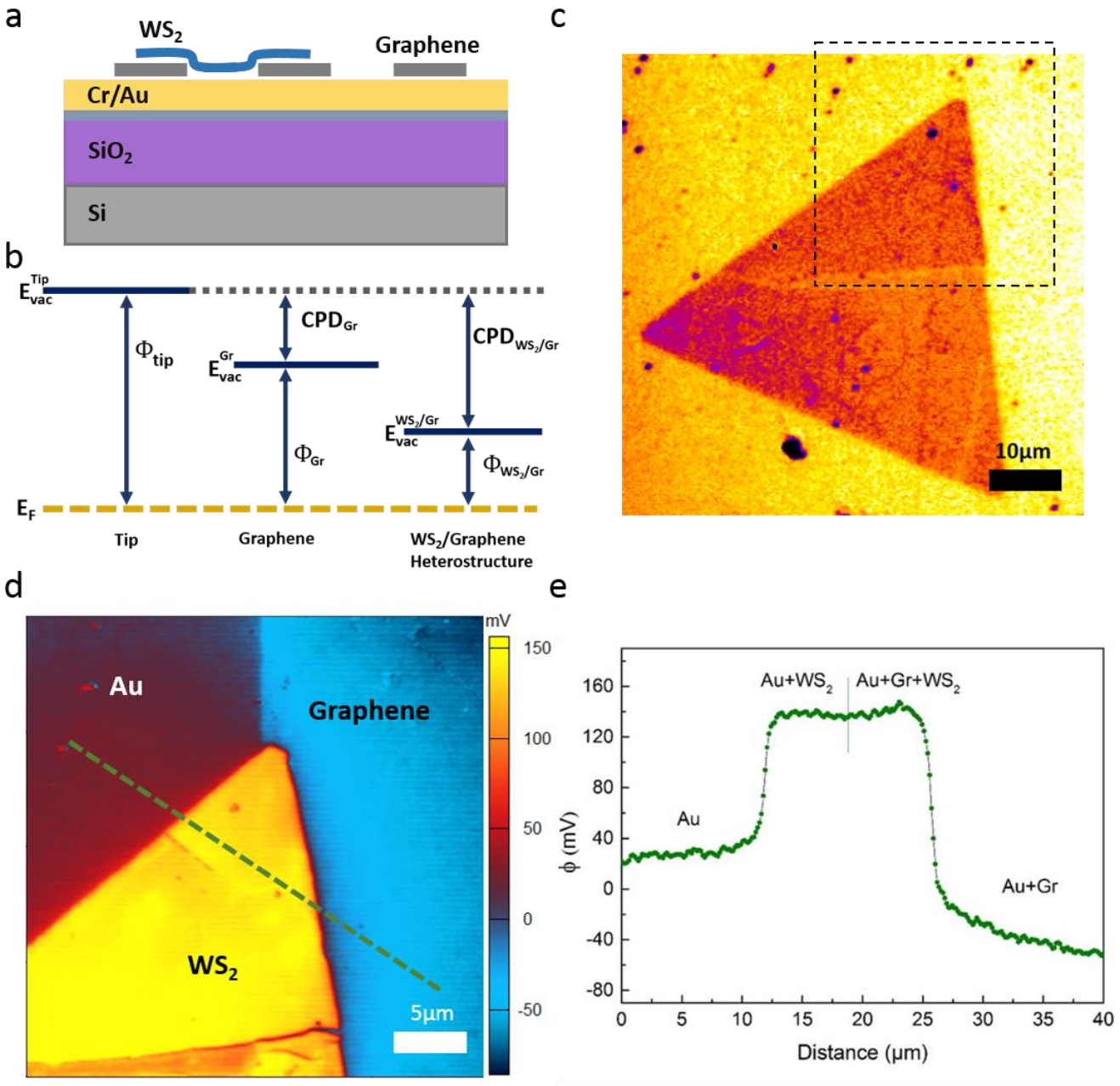

Figure 5. KPM Surface potential map of graphene/WS_2 heterostructure on Au. (a) Side view schematic of heterostructure sample for KPM. (b) Schematic of energy band diagrams of graphene and graphene/WS_2 heterostructure, relative to KPM tip, depicting CPD and work function. (c) Optical image with added contrast of graphene/WS_2 heterostructure on gold electrode. (d) KPM map of the surface potential of the Au, WS_2 and graphene (e) Line scan of surface potential across Au, WS_2 and graphene.

In Figure 6 we demonstrate further n-doping of graphene by photo-irradiation of the heterostructured region using a 532 nm laser with variable power. The field effect behavior of the graphene transistors with partial WS_2 coverage is highly responsive to the input laser power (Figure 6c and 6d). The two Dirac points, which are attributed to the WS_2-doped region and uncovered graphene respectively, shift at different rates with increasing laser power, resulting in a split of the two Dirac points (Figure 6d). This suggests that a further n-doping effect can be induced from photo-excited states at the WS_2/graphene interface along with initial charge transfer that occurs upon simple contact between the two materials. The photoinduced doping of graphene is attributed to charge separation of photo-generated excitons at the WS_2/graphene interface, with holes confined in the WS_2 while the electrons are transferred into graphene. This agrees with prior reports on interlayer coupling and charge transfer in other 2D crystal vertical heterostructures.[41–43] This result also supports the observation of PL quenching with concomitant reduction in the ratio of trion/exciton emission for WS_2 on graphene, seen in Figure 1 and 2. Placing WS_2 on graphene causes an initial charge transfer of electrons from WS_2 to graphene, which reduces the level of n-doping in WS_2 and thus reduces trion emission relative to excitonic emission. A decrease in the p-doping of graphene in FET measurements is also an effect of this. Upon photo-irradiation, excitons in WS_2 are split, with electrons transferred to graphene and holes remaining in the WS_2. The splitting of the exciton causes a reduction in the quantum yield of the direct excitonic recombination process in WS_2 and further reduction in the p-doping levels of graphene.[41]

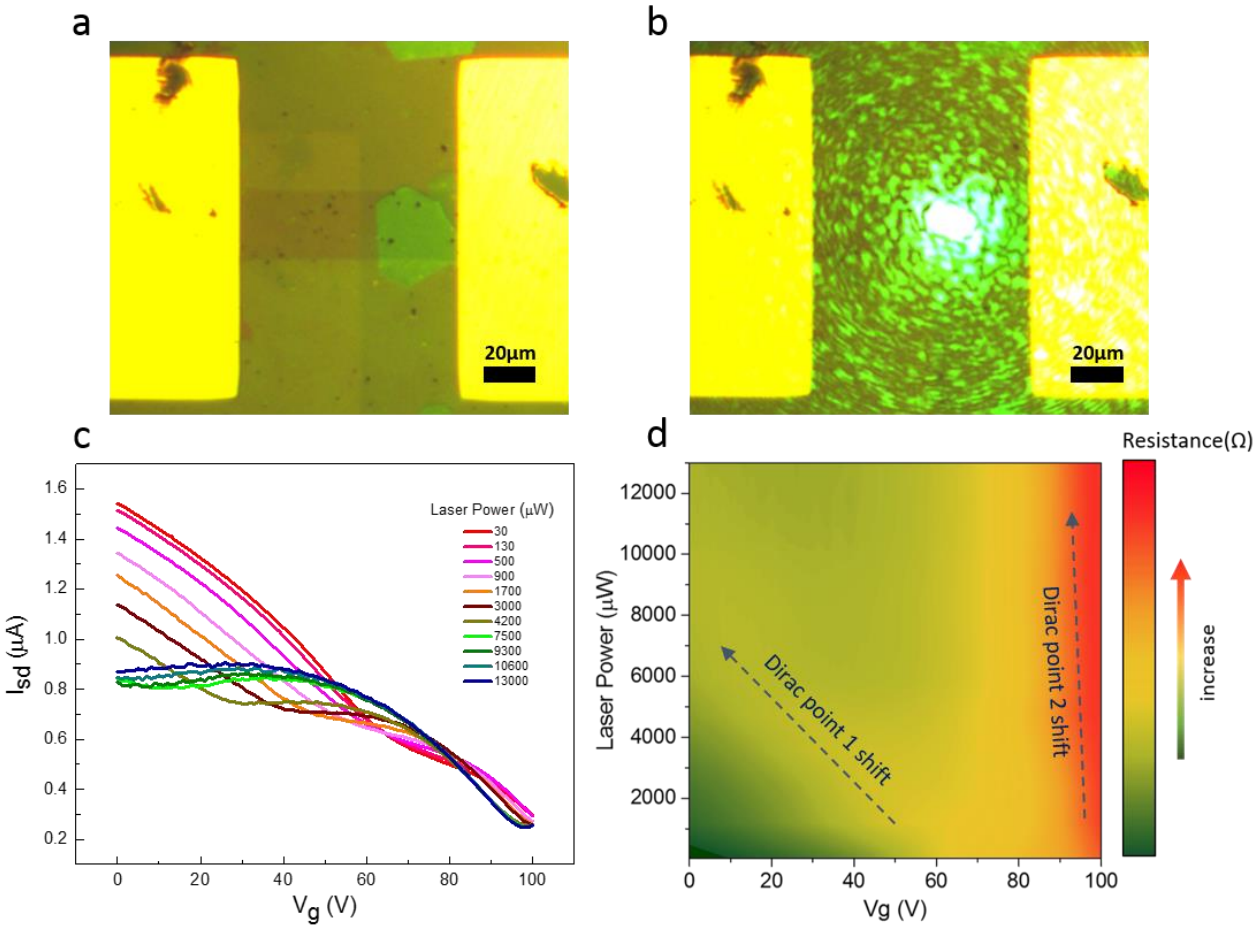

Figure 6. Photo-irradiation of WS_2/graphene interface. (a) Optical image of a graphene transistor partially covered by WS_2. (b) Optical image of device illuminated with 532 nm laser. The laser is centered at the edge of the WS_2 domain so that both graphene and heterostructured region are illuminated. (c) Field effect measurement device under increasing laser power. (d) Contour plot of the resistance of graphene channel in response to the illumination power and applied back-gate voltage.

Conclusion

In summary, we have created graphene/WS_2 vertical heterostructures using all CVD grown materials and characterized the interlayer coupling of the vdW crystals using optical spectroscopy and electronic measurements. Strong quenching of the PL is observed for WS_2 on graphene, indicative of strong interactions between the two layers, which is also supported by the electronic transport measurements of graphene and the photoinduced doping effect. By only partially covering graphene with WS_2, it is possible to locally

modulate the doping of graphene and construct graphene FETs with double-Dirac points. Our work shows that CVD grown WS_2 can be transferred on top of the graphene and still exhibit strong interactions in both optical and electronic properties. The doping effect can be further modulated by controlling the laser power illuminating the heterostructure. This opens up the possibility of large scale device fabrication based on all CVD materials that cannot be achieved with 2D materials isolated by mechanical exfoliation. Our findings can serve as ground work for novel photodetectors using surface charge transfer between 2D crystals.

Experimental Methods

CVD Synthesis of monolayer WS_2

Monolayer WS_2 was grown on 90nm SiO_2/Si substrate using our previously reported method with slight modifications of the CVD set up.[29,44] The two precursors, sulphur powder (400 mg of purum grade 99.5%) and WO_3 (200 mg of puriss grade 99.9%) are placed separately in a double-walled-quartz-tube. Sulphur and WO_3 powder were positioned in the external and internal tube respectively and heated by two furnace systems. Vaporized precursors are brought to the reaction zone by argon gas flow, where WO_3 undergoes sulfurization. The as-grown WS_2 samples were fast cooled as soon as the reaction is completed.

CVD Synthesis of monolayer Graphene

Monolayer graphene was grown using our previously reported method involving Cu as catalyst and tungsten as substrate.[30] Cu and W were cut into 1 cm^2 pieces and rinsed in acetone and IPA. Hydrochloric acid was applied to Cu before rinsing to eliminate the oxide layer. Cu was mounted on W and placed in the furnace. 100 sccm of Hydrogen (25%) and 200 sccm of Argon was used to anneal the sample at 1090 for 30 min before growth. Graphene was grown on the melted Cu with a flow of 200 sccm Argon, 30 sccm Hydrogen (25%) and 10 sccm of Methane (1%) for 90 min, subsequently followed by a secondary growth

process at 1060 ˚C for 30 min. The sample was subsequently removed from the heating zone and cooled to room temperature.

Transfer of Graphene and WS_2 domains

The as-grown CVD samples were first spin-coated with a poly(methyl methacrylate) (PMMA) scaffold (8 wt% in anisole, 495k molecular weight) at 4500 rpm for 60 s and cured at 150 ˚C for 15 min. W substrate of the Graphene sample was electrochemically etched in NaOH (2 M) by connecting a 2.4 V on the sample and using a Cu foil as anode. The PMMA/Graphene film was then separated from Cu substrate by $(NH_4)_2S_2O_8$ etching (0.1 M). The PMMA/WS_2 film was separated from the SiO_2/Si substrate by KOH etching (1 M) at 60 ˚C. The floating PMMA/Graphene and PMMA/WS_2 films were carefully transferred several times into deionized water to dilute residual contaminants. The films were subsequently transferred onto Si chip and baked at 150 ˚C for 30 min for sample adhesion.

Device fabrication

JEOL 5500 FS EBL system was used to pattern contacts in a bilayer PMMA resist. A thermal evaporator was used to deposit Cr/Au (10 nm/80 nm) electrodes onto a 300nm SiO_2/Si substrate, followed by liftoff in acetone at 45 ˚C. Graphene/PMMA film was scooped and transferred onto the Si chip with pre-patterned electrodes and baked overnight at 180 ˚C for better contact. Graphene were subsequently patterned using EBL with negative resist and oxygen plasma etching to define the graphene channels with a length and width of 100 µm and 25 µm respectively. The sample was soaked in hot acetone to remove residual PMMA and negative resist. Lastly, WS_2/PMMA film was transferred onto the sample and baked at 150 ˚C for 30 min. PMMA was removed in hot acetone.

Electrical Characterization

Heavily p-doped silicon was used as back gate. The field effect of graphene channels was characterized using a HP4156 Semiconductor Parameter Analyzer and probe station. A total of 220 devices were characterized under ambient conditions.

Optical Characterization

PL spectroscopy was carried out using a LabRam Aramis Raman Spectrometer. Samples are illuminated with a 532 nm laser of 200 μW, through a ×50 objective lens with a spot size of ~2 μm.

Kelvin Probe Microscopy (KPM) Characterization

KPM was used to probe the surface potential of WS_2 and Graphene with a gold substrate as reference. KPM measurements have been performed on an Asylum Research MFP-3D atomic force microscope with a Cr/Pt plated cantilever with a spring constant of 2.17 N/m and resonance frequency of 67.12 kHz. A standard two-pass procedure is used to map the topography and KPM information, in which each measurement of the topography line in the amplitude-modulated non-contact mode is followed by the acquisition of a KPM line 50 nm above the topography trace.

Supporting Information

The Supporting Information is available free of charge on the ACS Publications website at DOI:

Raman, PL and TEM of 2D materials used for device, fitting model with e-h puddle, statistics of residual charge carrier concentration of devices, comparison of doping effects of WS_2 with/without gold connection.

Acknowledgements

JHW thanks the support from the Royal Society. H. Tan thanks Yayasan Khazanah for funding the Merdeka Scholarship.

References

(1) Schwierz, F. Graphene Transistors. *Nat. Nanotechnol.* **2010**, *5*, 487–496.

(2) Wang, Q. H.; Kalantar-Zadeh, K.; Kis, A.; Coleman, J. N.; Strano, M. S. Electronics and Optoelectronics of Two-Dimensional Transition Metal Dichalcogenides. *Nat. Nanotechnol.* **2012**, *7*, 699–712.

(3) Georgiou, T.; Jalil, R.; Belle, B. D.; Britnell, L.; Gorbachev, R. V; Morozov, S. V; Kim, Y.-J.; Gholinia, A.; Haigh, S. J.; Makarovsky, O.; Eaves, L.; Ponomarenko, L. A.; Geim, A. K.; Novoselov, K. S.; Mishchenko, A. Vertical Field-Effect Transistor Based on Graphene-WS2 Heterostructures for Flexible and Transparent Electronics. *Nat. Nanotechnol.* **2013**, *8*, 100–103.

(4) Sire, C. D. Flexible Gigahertz Transistors Derived from Solution-Based Single-Layer Graphene. *Nano Lett.* **2012**, *12*, 1184–1188.

(5) Roy, T.; Tosun, M.; Kang, J. S.; Sachid, A. B.; Desai, S. B.; Hettick, M.; Hu, C. C.; Javey, A. Field-Effect Transistors Built from All Two-Dimensional Material Components. *ACS Nano* **2014**, *8*, 6259–6264.

(6) Lee, C.-H.; Lee, G.-H.; van der Zande, A. M.; Chen, W.; Li, Y.; Han, M.; Cui, X.; Arefe, G.; Nuckolls, C.; Heinz, T. F.; Guo, J.; Hone, J.; Kim, P. Atomically Thin P–N Junctions with van Der Waals Heterointerfaces. *Nat. Nanotechnol.* **2014**, *9*, 676–681.

(7) Novoselov, K. S.; Geim, A. K.; Morozov, S. V; Jiang, D.; Zhang, Y.; Dubonos, S. V; Grigorieva, I. V; Firsov, A. A. Electric Field Effect in Atomically Thin Carbon Films. *Sci.* **2004**, *306* , 666–669.

(8) Kim, K. S.; Zhao, Y.; Jang, H.; Lee, S. Y.; Kim, J. M.; Kim, K. S.; Ahn, J.-H.; Kim, P.; Choi, J.-Y.; Hong, B. H. Large-Scale Pattern Growth of Graphene Films for Stretchable Transparent Electrodes. *Nature* **2009**, *457*, 706–710.

(9) Liu, N.; Tian, H.; Schwartz, G.; Tok, J. B.-H.; Ren, T.-L.; Bao, Z. Large-Area, Transparent, and Flexible Infrared Photodetector Fabricated Using P-N Junctions Formed by N-Doping Chemical Vapor Deposition Grown Graphene. *Nano Lett.* **2014**, *14*, 3702–3708.

(10) Mak, K. F.; Lee, C.; Hone, J.; Shan, J.; Heinz, T. F. Atomically Thin MoS2: A New Direct-Gap Semiconductor. *Phys. Rev. Lett.* **2010**, *105*, 136805.

(11) Splendiani, A.; Sun, L.; Zhang, Y.; Li, T.; Kim, J.; Chim, C.-Y.; Galli, G.; Wang, F. Emerging Photoluminescence in Monolayer MoS2. *Nano Lett.* **2010**, *10*, 1271–1275.

(12) Gutiérrez, H. R.; Perea-López, N.; Elías, A. L.; Berkdemir, A.; Wang, B.; Lv, R.; López-Urías, F.; Crespi, V. H.; Terrones, H.; Terrones, M. Extraordinary Room-Temperature Photoluminescence in Triangular WS2 Monolayers. *Nano Lett.* **2013**, *13*, 3447–3454.

(13) Britnell, L.; Gorbachev, R. V; Jalil, R.; Belle, B. D.; Schedin, F.; Mishchenko, A.; Georgiou, T.; Katsnelson, M. I.; Eaves, L.; Morozov, S. V; Peres, N. M. R.; Leist, J.; Geim, A. K.; Novoselov, K. S.; Ponomarenko, L. A. Field-Effect Tunneling Transistor Based on Vertical Graphene Heterostructures. *Science* **2012**, *335*, 947–950.

(14) Loan, P. T. K.; Zhang, W.; Lin, C.-T.; Wei, K.-H.; Li, L.-J.; Chen, C.-H. Graphene/MoS2 Heterostructures for Ultrasensitive Detection of DNA Hybridisation. *Adv. Mater.* **2014**, *26*, 4838–4844.

(15) Roy, K.; Padmanabhan, M.; Goswami, S.; Sai, T. P.; Ramalingam, G.; Raghavan, S.; Ghosh, A. Graphene-MoS2 Hybrid Structures for Multifunctional Photoresponsive Memory Devices. *Nat. Nanotechnol.* **2013**, *8*, 826–830.

(16) Pospischil, A.; Furchi, M. M.; Mueller, T. Solar-Energy Conversion and Light Emission in an

Atomic Monolayer P-N Diode. *Nat. Nanotechnol.* **2014**, *9*, 257–261.

(17) Huo, N.; Wei, Z.; Meng, X.; Kang, J.; Wu, F.; Li, S.-S.; Wei, S.-H.; Li, J. Interlayer Coupling and Optoelectronic Properties of Ultrathin Two-Dimensional Heterostructures Based on Graphene, MoS2 and WS2. *J. Mater. Chem. C* **2015**, *3*, 5467–5473.

(18) Rathi, S.; Lee, I.; Lim, D.; Wang, J.; Ochiai, Y.; Aoki, N.; Watanabe, K.; Taniguchi, T.; Lee, G.-H.; Yu, Y.-J.; Kim, P.; Kim, G.-H. Tunable Electrical and Optical Characteristics in Monolayer Graphene and Few-Layer MoS2 Heterostructure Devices. *Nano Lett.* **2015**, *15*, 5017–5024.

(19) Williams, J. R.; Dicarlo, L.; Marcus, C. M. Quantum Hall Effect in a Gate-Controlled P-N Junction of Graphene. *Science* **2007**, *317*, 638–641.

(20) Özyilmaz, B.; Jarillo-Herrero, P.; Efetov, D.; Abanin, D.; Levitov, L.; Kim, P. Electronic Transport and Quantum Hall Effect in Bipolar Graphene P-N-P Junctions. *Phys. Rev. Lett.* **2007**, *99*, 166804.

(21) Chiu, H.-Y.; Perebeinos, V.; Lin, Y.-M.; Avouris, P. Controllable P-N Junction Formation in Monolayer Graphene Using Electrostatic Substrate Engineering. *Nano Lett.* **2010**, *10*, 4634–4639.

(22) Wang, X.; Jiang, X.; Wang, T.; Shi, J.; Liu, M.; Zeng, Q.; Cheng, Z.; Qiu, X. Electrically Configurable Graphene Field-Effect Transistors with a Graded-Potential Gate. *Nano Lett.* **2015**, *15*, 3212–3216.

(23) Brenner, K.; Murali, R. Single Step, Complementary Doping of Graphene. *Appl. Phys. Lett.* **2010**, *96*, 063104.

(24) Usachov, D.; Vilkov, O.; Grüneis, A.; Haberer, D.; Fedorov, A.; Adamchuk, V. K.; Preobrajenski, A. B.; Dudin, P.; Barinov, A.; Oehzelt, M.; Laubschat, C.; Vyalikh, D. V. Nitrogen-Doped Graphene: Efficient Growth, Structure, and Electronic Properties. *Nano Lett.* **2011**, *11*, 5401–5407.

(25) Xiang, D.; Han, C.; Wu, J.; Zhong, S.; Liu, Y.; Lin, J.; Zhang, X.-A.; Ping Hu, W.; Özyilmaz, B.; Neto, A. H. C.; Wee, A. T. S.; Chen, W. Surface Transfer Doping Induced Effective Modulation on Ambipolar Characteristics of Few-Layer Black Phosphorus. *Nat. Commun.* **2015**, *6*, 6485.

(26) Lemme, M. C.; Koppens, F. H. L.; Falk, A. L.; Rudner, M. S.; Park, H.; Levitov, L. S.; Marcus, C. M. Gate-Activated Photoresponse in a Graphene P-N Junction. *Nano Lett.* **2011**, *11*, 4134–4137.

(27) Sun, D.; Aivazian, G.; Jones, A. M.; Ross, J. S.; Yao, W.; Cobden, D.; Xu, X. Ultrafast Hot-Carrier-Dominated Photocurrent in Graphene. *Nat. Nanotechnol.* **2012**, *7*, 114–118.

(28) Freitag, M.; Low, T.; Xia, F.; Avouris, P. Photoconductivity of Biased Graphene. *Nat. Photonics* **2012**, *7*, 53–59.

(29) Rong, Y.; Fan, Y.; Leen Koh, A.; Robertson, A. W.; He, K.; Wang, S.; Tan, H.; Sinclair, R.; Warner, J. H. Controlling Sulphur Precursor Addition for Large Single Crystal Domains of WS2. *Nanoscale* **2014**, *6*, 12096–12103.

(30) Fan, Y.; He, K.; Tan, H.; Speller, S.; Warner, J. H. Crack-Free Growth and Transfer of Continuous Monolayer Graphene Grown on Melted Copper. *Chem. Mater.* **2014**, *26*, 4984–4991.

(31) Bhanu, U.; Islam, M. R.; Tetard, L.; Khondaker, S. I. Photoluminescence Quenching in Gold - MoS2 Hybrid Nanoflakes. *Sci. Rep.* **2014**, *4*, 5575.

(32) Chernikov, A.; Berkelbach, T. C.; Hill, H. M.; Rigosi, A.; Li, Y.; Aslan, O. B.; Reichman, D. R.; Hybertsen, M. S.; Heinz, T. F. Exciton Binding Energy and Nonhydrogenic Rydberg Series in Monolayer WS2. *Phys. Rev. Lett.* **2014**, *113*, 76802.

(33) Mitioglu, A.; Plochocka, P.; Jadczak, J.; Escoffier, W.; Rikken, G.; Kulyuk, L.; Maude, D.

Optical Manipulation of the Exciton Charge State in Single-Layer Tungsten Disulfide. *Phys. Rev. B* **2013**, *88*, 245403.

(34) Zhu, B.; Chen, X.; Cui, X. Exciton Binding Energy of Monolayer WS2. *Sci. Rep.* **2015**, *5*.

(35) Nistor, R. A.; Kuroda, M. A.; Maarouf, A. A.; Martyna, G. J. Doping of Adsorbed Graphene from Defects and Impurities in SiO2 Substrates. *Phys. Rev. B - Condens. Matter Mater. Phys.* **2012**, *86*, 1–5.

(36) Kretinin, A. V.; Cao, Y.; Tu, J. S.; Yu, G. L.; Jalil, R.; Novoselov, K. S.; Haigh, S. J.; Gholinia, A.; Mishchenko, A.; Lozada, M.; Georgiou, T.; Woods, C. R.; Withers, F.; Blake, P.; Eda, G.; Wirsig, A.; Hucho, C.; Watanabe, K.; Taniguchi, T.; Geim, A. K.; Gorbachev, R. V. Electronic Properties of Graphene Encapsulated with Different Two-Dimensional Atomic Crystals. *Nano Lett.* **2014**, *14*, 3270–3276.

(37) Haigh, S. J.; Gholinia, A.; Jalil, R.; Romani, S.; Britnell, L.; Elias, D. C.; Novoselov, K. S.; Ponomarenko, L. A.; Geim, A. K.; Gorbachev, R. Cross-Sectional Imaging of Individual Layers and Buried Interfaces of Graphene-Based Heterostructures and Superlattices. *Nat. Mater.* **2012**, *11*, 764–767.

(38) Wang, Y.; Geer, R. E. Surface Potential Measurements of Reconfigurable P-N Junctions in Graphene. *ECS Trans.* **2012**, *45* , 31–37.

(39) Tosun, M.; Fu, D.; Desai, S. B.; Ko, C.; Seuk Kang, J.; Lien, D.-H.; Najmzadeh, M.; Tongay, S.; Wu, J.; Javey, A. MoS2 Heterojunctions by Thickness Modulation. *Sci. Rep.* **2015**, *5*, 10990.

(40) Chen, K.; Wan, X.; Wen, J.; Xie, W.; Kang, Z.; Zeng, X.; Chen, H.; Xu, J.-B. Electronic Properties of MoS2–WS2 Heterostructures Synthesized with Two-Step Lateral Epitaxial Strategy. *ACS Nano* **2015**, *9*, 9868–9876.

(41) Hong, X.; Kim, J.; Shi, S.-F.; Zhang, Y.; Jin, C.; Sun, Y.; Tongay, S.; Wu, J.; Zhang, Y.; Wang, F. Ultrafast Charge Transfer in Atomically Thin MoS2/WS2 Heterostructures. *Nat. Nanotechnol.* **2014**, *9*, 682–686.

(42) Ju, L.; Velasco, J.; Huang, E.; Kahn, S.; Nosiglia, C.; Tsai, H.-Z.; Yang, W.; Taniguchi, T.; Watanabe, K.; Zhang, Y.; Zhang, G.; Crommie, M.; Zettl, A.; Wang, F. Photoinduced Doping in Heterostructures of Graphene and Boron Nitride. *Nat. Nanotechnol.* **2014**, *9*, 348–352.

(43) Konstantatos, G.; Badioli, M.; Gaudreau, L.; Osmond, J.; Bernechea, M.; de Arquer, F. P. G.; Gatti, F.; Koppens, F. H. L. Hybrid Graphene-Quantum Dot Phototransistors with Ultrahigh Gain. *Nat Nano* **2012**, *7*, 363–368.

(44) Rong, Y.; He, K.; Pacios, M.; Robertson, A. W.; Bhaskaran, H.; Warner, J. H. Controlled Preferential Oxidation of Grain Boundaries in Monolayer Tungsten Disulfide for Direct Optical Imaging. *ACS Nano* **2015**, *9*, 3695–3703.

TOC graphics